HHS Public Access

Author manuscript

J Magn Reson Imaging. Author manuscript; available in PMC 2017 January 01.

Published in final edited form as:

J Magn Reson Imaging. 2016 January ; 43(1): 107–114. doi:10.1002/jmri.24962.

4D Flow MRI and T1-Mapping: Assessment of Altered Cardiac Hemodynamics and Extracellular Volume Fraction in Hypertrophic Cardiomyopathy

Pim van Ooij, PhD[1], **Bradley D. Allen, MD**[1], **Carla Contaldi, MD**[2], **Julio Garcia, PhD**[1], **Jeremy Collins, MD**[1], **James Carr, MD**[1], **Lubna Choudhury, MD**[2], **Robert O. Bonow, MD, MS**[2], **Alex J. Barker, PhD**[1], and **Michael Markl, PhD**[1,3]

[1]Department of Radiology, Feinberg School of Medicine, Northwestern University, Chicago, IL, USA

[2]Department of Medicine-Cardiology, Northwestern University, Chicago, IL, USA

[3]Department of Biomedical Engineering, McCormick School of Engineering, Northwestern University, Chicago, IL, USA

Abstract

Purpose—Hypertrophic cardiomyopathy (HCM) is associated with altered hemodynamics in the left ventricular out flow tract (LVOT) and myocardial tissue abnormalities such as fibrosis. The aim of this study was to quantify changes in LVOT 3D hemodynamics and myocardial extracellular volume fraction (ECV, measure of fibrosis) and to investigate relationships between elevated flow metrics and left ventricular (LV) tissue abnormalities.

Methods and Results—Cardiac MRI including 4D flow (field strength=1.5T, resolution=2.1–4.0×2.1–4.0×2.5–3.2mm^3; venc=150–250cm/s; TE/TR/FA=2.2–2.5ms/4.6–4.9ms/15°) for the in-vivo assessment of 3D blood flow velocities with full coverage of the LVOT was applied in 35 patients with HCM (54±15 years) and 10 age matched healthy controls (45±14 years). In addition, pre- and post-contrast myocardial T1-mapping (resolution=2.3×1.8mm, slice thickness=8mm, TE/TR-FA=1.0–1.1ms/2.0–2.2ms/35°) of the LV (basal, mid-ventricular, apical short axis) was performed in a subgroup of 23 HCM patients. Analysis included the segmentation of the LVOT and quantification of peak systolic LVOT pressure gradients and rate of viscous energy loss $E_L^{'}$ as well as left ventricular ECV.

Results—HCM patients demonstrated significantly elevated peak systolic LVOT pressure gradients (21±16mmHg vs. 9±2mmHg) and energy loss $E_L^{'}$ (3.8±2.5mW vs. 1.5±0.7mW, P<0.005) compared to controls. There was a significant relationship between increased LV fibrosis (ECV) with both elevated pressure gradients (R^2=0.44, P<0.001) and energy loss $E_L^{'}$ (R^2=0.46, P<0.001).

Corresponding author: Michael Markl, Ph.D., Department of Radiology, Northwestern University, 737 N. Michigan Avenue Suite 1600, Chicago, Illinois 60611, USA, Phone: +1 312-695-1799, michael.markl@northwestern.edu.

Conclusions—The integration of 4D-flow and T_1-mapping-MRI allowed for the evaluation of tissue and flow abnormalities in HCM patients. Our findings suggest a mechanistic link between abnormal LVOT flow, increased LV loading, and adverse myocardial remodeling in HCM.

Keywords

Hypertrophic cardiomyopathy; 4D flow MRI; energy loss; T1-mapping; extracellular volume fraction; fibrosis; pressure gradient

INTRODUCTION

Hypertrophic cardiomyopathy (HCM) is a complex cardiac disease with an incidence of 0.2% to 0.5% (1,2) associated with sudden cardiac death and progressive heart failure (3). In many cases, the combination of systolic anterior motion (SAM) of the mitral valve and septal thickening can dynamically obstruct the LV outflow tract (LVOT) and result in increased systolic LVOT pressure gradients and thus elevated ventricular loading(4–7). In addition, HCM can result in left ventricular (LV) abnormalities including myocardial thickening(8), fibrosis (9), and scarring (10). These findings suggest a structure-function relationship between altered LVOT hemodynamics, increased LV loading and structural remodeling of the LV (fibrosis, scar) inherent to HCM.

Current diagnostic tools such as Doppler echocardiography can reliably evaluate LV wall thickness, peak velocity in the LVOT and the presence of SAM in HCM (11),(12). However, Doppler echocardiography cannot assess the full extent of complex changes in LVOT hemodynamics and myocardial tissue abnormalities such as fibrosis (13,14). Recent developments in MRI permit the evaluation of cardiovascular hemodynamics with full coverage of the heart using 4D flow MRI, which can visualize complex helical LVOT 3D flow patterns and quantify LVOT obstruction in the presence of high velocity systolic outflow jets(15,16). The use of this technique also allows for computation of hemodynamic energy loss (17) caused by complex non-turbulent 3D blood flow (18,19) as an alternative measure of increased LV afterload. In addition, the quantification of myocardial T_1 relaxation times before and after the administration of gadolinium contrast agent has been used to assess cardiac tissue abnormalities (20). Specifically, pre- and post-contrast T_1-mapping techniques can be employed to quantify myocardial extracellular volume fraction (ECV) as marker of diffuse interstitial fibrosis (21–24). Previous studies have found elevated diffuse fibrosis (25) and ECV (26) in myocardial tissue in HCM patients.

However, the interrelationship between tissue abnormalities and altered LVOT hemodynamics is still poorly understood. The aim of this study was therefore to employ both 4D flow MRI and pre- and post-contrast T_1-mapping to investigate associations between abnormal LVOT hemodynamics (peak systolic pressure gradient and energy loss) and structural myocardial abnormalities (ECV). We hypothesized that there is a significant relationship between altered LVOT hemodynamics and LV tissue abnormalities in patients with HCM.

METHODS

Study Cohort

Thirty-five patients (54±15 years, range: 18–80 years, 25 men) with asymmetric basal-septal hypertrophy based on echocardiography were referred for cardiac MR as part of HCM assessment. Additionally, 10 healthy volunteers (45±14 years, range: 21–69 years, 6 men, age difference P-value = 0.11) were included. Patients were included in accordance with an IRB protocol which permitted retrospective chart review. Informed consent was obtained from all healthy volunteers.

Magnetic Resonance Imaging

All patients underwent a standard-of-care cardiac MRI exam on a 1.5T MRI system (Magnetom Avanto and Aera, Siemens, Germany) including ECG gated time-resolved (CINE) cardiac MRI for the evaluation of cardiac dimensions and function.

For the assessment of aortic blood flow, time-resolved 3D phase-contrast MRI with three-directional velocity encoding (4D flow MRI) was employed to measure 3D blood flow velocities with full volumetric coverage of the left ventricle, LVOT, and ascending aorta. 4D flow data were acquired in 3-chamber orientation (24 subjects) or in a sagittal oblique volume (11 subjects). 4D flow MRI was acquired during free breathing using respiratory and prospective ECG gating as described previously(27). Pulse sequence parameters were as follows: spatial resolution = 2.1–4.0×2.1–4.0×2.5–3.2mm^3; temporal resolution = 37–40ms; field of view = 255–340mm×255–360mm^2, slab thickness = 65–132mm, velocity sensitivity (venc) = 150–250cm/s; echo time (TE) = 2.2–2.5ms; repetition time (TR) = 4.6–4.9ms; flip angle = 15°. All 4D flow MRI scans were acquired with parallel imaging (GRAPPA) with a reduction factor of R = 2 and 24 reference lines (net acceleration factor = 1.7).

T_1-mapping was performed using a modified Look-Locker inversion recovery (MOLLI) technique as described previously by Messroghli and co-workers, utilizing a 17 heart beat acquisition comprising three Look-Locker cycles, separated by recovery periods of three heart beats (28). The first and second Look-Locker cycles comprised three heartbeats and the third comprised five heartbeats. Data for each slice (base, mid, apex) were acquired during breath holding pre- and 10–25 minutes following the intravenous administration of a contrast agent bolus. Imaging reconstruction included motion correction of the MOLLI images with different inversion times, and the calculation of parametric LV T_1 maps as described previously (29,30). T1 mapping parameters were as follows: spatial resolution (pixel size)=2.3×1.8mm, slice thickness=8mm, TE/TR=1.0–1.1ms/2.0–2.2ms; flip angle=35°. Gadopentetate dimeglumine (Magnevist, Bayer Pharmaceuticals, Whippany, NJ) was administered as a bolus infusion at a dose of 0.1mmol/kg. Patient hematocrit was collected within 48 hours of the cardiac MRI exam.

Data Analysis - SAM and LVOT Dimensions

End-diastolic septal thickness, end-diastolic septum/free wall ratio and presence of SAM were evaluated and quantified on 3-chamber CINE images. End-diastolic LVOT diameter

was defined as the average of the outflow diameter measured in 3-camber and LVOT orientation.

Data Analysis - LVOT Flow, Pressure Gradient, and Energy Loss

Data preprocessing included noise filtering and correction for eddy currents, Maxwell terms, and velocity aliasing, as previously described by Bock et al. (31). 3D phase contrast (PC) MR angiogram (MRA) images, weighted for the systolic time frames were derived from 4D flow data by multiplication of the phase contrast magnitude images with the absolute velocity images. The PC-MRA images were subsequently averaged over all cardiac time frames and used to semi-automatically segment the LVOT region using a commercial software package (MIMICS, Materialise, Leuven, Belgium). 3D blood flow visualization (Ensight, CEI, Apex, NC, USA) using streamlines was employed to depict peak systolic blood flow patterns inside the 3D LVOT segmentation. Peak systole was defined as the cardiac time frame with the highest mean LVOT velocity. The maximum blood flow velocity in the LVOT at peak systole was automatically detected and a 4D flow MRI-derived LVOT pressure gradient was calculated using the simplified Bernoulli equation (32).

The rate of energy loss due to viscous dissipation ($E_L^{'}$) in the segmented LVOT volume was calculated at peak systole using a recently reported approach (19). Briefly, $E_L^{'}$ was derived using:

$$E_L^{'}=\mu\sum_{i=1}^{N} V_i\phi_v \quad (1)$$

where μ is the dynamic viscosity of blood (3.2 cP), N is the number of voxels, V is the volume of a voxel and ϕ_v is the viscous dissipation as given by (33):

$$\phi_v=\frac{1}{2}\sum_i\sum_j\left[\left(\frac{\partial v_i}{\partial x_j}+\frac{\partial v_j}{\partial x_i}\right)-\frac{2}{3}(\nabla.\boldsymbol{v})\,\delta_{ij}\right]^2 \quad where \quad \begin{matrix}\delta_{ij}=1\ for\ i=j\\ \delta_{ij}=0\ for\ i\neq j\end{matrix} \quad (2)$$

where i and j are the principal directions x, y, z and v is the velocity field as measured by 4D flow MRI and filtered by a 3×3 median filter to reduce noise (19). The regional rate of peak systolic energy loss was visualized using a maximum intensity projection (MIP) of the dissipation field (ϕ_v) and the cumulative $E_L^{'}$ was calculated by summing all voxels in the 3D segmentation (equation 1).

Inter- and Intra-Observer Variability

To test the influence of semi-automatic 3D LVOT segmentation on Bernoulli pressure gradient estimation and calculation of $E_L^{'}$, data analysis was performed by two observers (PvO and JG) with both two months of experience with the segmentation process for a subset of 18 HCM patients and 7 controls (blinded to the results of the first observer) and repeated by the first observer.

Data Analysis - T_1-Mapping and Extracellular Volume Fraction

Epi- and endocardial LV contours (base, mid, apex) were manually delineated (PvO and CC with one month and two months, respectively, of experience with the T1-mapping process) in the pre- and post-contrast T_1 maps using Q Mass MR (version 7.5, Medis Inc, Leiden, The Netherlands). In addition, regions of interest were drawn in the blood pool, in the septum, and in the free wall. In all regions, myocardial ECV was calculated using (34,35):

$$ECV = \frac{T_{1,post} - T_{1,pre_{blood}}}{T_{1,post} - T_{1,pre_{myocardium}}} \times (1 - hematrocrit) \quad (3)$$

where $T_{1,pre}$ and $T_{1,post}$ represent the T_1 values before and after Gd-contrast agent administration. In addition, ECV of basal, mid and apical locations were averaged to yield left ventricular ECV.

Statistical Analysis

Results are expressed as mean±standard deviation (SD). Differences between groups were assessed using Wilcoxon rank sum and Kruskal-Wallis tests as appropriate. Linear regression was performed to assess correlations between variables of interest and the coefficient of correlation (R^2) was calculated. If one variable was discrete and one was continuous, a point biserial coefficient of correlation R^2 was calculated. $P<0.05$ was considered statistically significant. Bland-Altman analysis was used to assess agreement between observers and the mean difference and limits of agreement (LOA, ±1.96 SD) were calculated.

RESULTS

Patient Characteristics

Patient characteristics are summarized in table 1. In all patients, 4D flow MRI for the in-vivo assessment of 3D blood flow velocities and calculation of LVOT pressure gradients and energy loss $E_L^{'}$ was successfully performed. In a subset of 23 patients (18 men, age = 53±16 years) pre- and post Gd-contrast T_1-mapping was performed and blood samples to calculate the hematocrit were acquired.

LVOT Pressure Gradient and $E_L^{'}$ in HCM Compared to Controls

Figure 1 shows representative examples of LVOT flow patterns including normal hemodynamics (figure 1a), abnormal helical flow in HCM without moderate obstruction (figure 1b), and substantially elevated flow velocities for HCM with severe LVOT obstruction (figure 1c). Compared to uniform outflow in the control subject, 3D streamlines highlight the presence of helical flow in HCM (figure 1b) and a central velocity jet (figure 1c, orange-red color indicating velocity > 2m/s) caused by outflow obstruction. Altered flow patterns in HCM patients were accompanied by increased peak systolic LVOT pressure gradients (33 mmHg and 63 mmHg) and energy loss $E_L^{'}$ (6 mW and 10 mW) compared to a healthy control (7 mmHg, and 2mW, respectively). Cumulative results for all 45 subjects are summarized in figure 2 and demonstrated significantly elevated peak systolic LVOT pressure

gradients (21±16mmHg versus 9±2mmHg, P<0.005) and energy loss $E_L^{'}$ (3.8±2.5mW versus 1.5±0.7mW, P<0.005) in HCM patients compared to age matched controls.

Relationship between LVOT Pressure Gradient, $E_L^{'}$ and ECV

Results of ECV quantification are summarized in table 2. Left ventricular, septal and free wall ECV were similar and demonstrated moderate but significant correlations with pressure gradients (R^2=0.34–0.44, P<0.001) as well as energy loss $E_L^{'}$ (R^2=0.31–0.46, P<0.001). The strongest associations were found for left ventricular ECV (figure 3a and b). In addition, univariate regression analysis revealed a strong and significant relationship between peak systolic LVOT pressure gradient and energy loss $E_L^{'}$ (figure 3c, R^2=0.86, P<0.001).

Relationship between LVOT Pressure Gradient, $E_L^{'}$ and Structural Parameters

Table 3 summarizes the results of linear regression analysis for peak systolic LVOT pressure gradients and energy loss $E_L^{'}$ as compared to septal thickness, septal/posterior wall thickness ratio, presence of SAM and LVOT diameter. Weak but significant relationships were found between peak systolic LVOT pressure gradients and presence of SAM and LVOT diameter.

Inter- and Intra-Observer Variability

Bland-Altman analysis showed good intra-observer (mean difference = −0.4mW, LOA= ±1.8mW) and inter-observer agreement (mean difference = −0.4mW, LOA=±1.3mW) for peak systolic LVOT energy loss $E_L^{'}$. Relative to mean $E_L^{'}$, intra-observer variability was 13% for controls and 17% for HCM patients. Inter-observer variability was 15% for both controls and HCM patients. For all subjects, intra- and inter-observer Bernoulli pressure gradients were identical except for one HCM patient (9% difference, 35 vs. 32 mm Hg).

DISCUSSION

The findings of this study demonstrate the potential of the combined application of pre- and post-contrast T_1-mapping and 4D flow MRI for the characterization of altered hemodynamics and myocardial ECV in patients with HCM. 4D flow MRI could detect altered pressure gradients and energy loss in patients compared to controls indicating significantly elevated LV loading in HCM. In addition, the integration of 4D flow MRI with T_1-mapping in a subset of 23 subjects allowed for the evaluation of structure (myocardial tissue) and function (blood flow) abnormalities in patients with HCM. ECV was significantly associated with elevated peak systolic LVOT pressure gradients or energy loss $E_L^{'}$.

These findings point towards a structure-function relationship between elevated LVOT pressure gradient or energy loss $E_L^{'}$ (i.e. increased LV loading) and adverse myocardial remodeling (i.e. elevated ECV). These findings are in good agreement with a recent study in a murine animal model of hypertension and LV pressure overload from trans-aortic

constriction by Coelho-Filho and co-workers (24). Results of this study demonstrated that ECV could track myocardial tissue remodeling that resulted from LV pressure overload.

Previous studies have shown that septal thickness is associated with LV fibrosis and sudden cardiac death(4–7). In our study cohort, however, changes in peak systolic pressure gradients or energy loss $E_L^{'}$ in HCM patients were only mildly associated with standard metrics of disease severity such as LVOT diameter, septal thickening or SAM. We speculate that altered hemodynamics in HCM may be the result of more complex descriptors than left ventricular and LVOT dimensions. Further longitudinal studies will be performed to further elucidate these structure-function relationships and their development and associations with disease progression and outcome.

In this study, changes in LVOT hemodynamics were quantified based on the commonly used pressure gradient estimation based on the simplified Bernoulli equation. In addition, the full volumetric coverage of the LVOT provided by 4D flow MRI allowed for the calculation of a recently introduced new metric for elevated ventricular loading: peak systolic energy loss $E_L^{'}$ (19). It is well known that pressure recovery is not accounted for with the Bernoulli equation, which can result in misclassification when assessing aortic valve stenosis(36). Therefore, we initially hypothesized that $E_L^{'}$ would allow for a better identification of patients with increased cardiac loading compared to Bernoulli based pressure gradient estimation. However, the results of our study showed that the peak systolic LVOT pressure gradient was highly correlated to energy loss $E_L^{'}$. $E_L^{'}$ did not offer any statistical advantage over peak systolic pressure gradient when assessing for a correlation with structural parameters. Additional studies are needed to perform a more systematic evaluation of differences in pressure gradients and energy loss and their relationship to LVOT out-flow patterns.

It should be noted that the addition of 4D flow MRI to standard clinical cardiac MRI protocols is still challenging due to limitations related to long total scan times on the order of 10–15 minutes and the need for often complex post-scan data analysis. Recent advances in imaging acceleration based on spatiotemporal undersampling methods such a k-t GRAPPA or compressed sensing are promising for further scan time reductions to achieve clinically more feasible scan times on the order of a few minutes (37–39). The analysis of 4D flow MRI data is typically based on multiple steps including corrections (eddy current induced phase offsets, velocity aliasing), 3D flow visualization, and extraction of metrics of cardiovascular hemodynamics (e.g. systolic pressure gradient). As a result, 4D flow post-processing can be time consuming and cumbersome and is not standardized across different institutions. Additional efforts are needed to develop streamlined 4D flow analysis workflows and tools to permit the more widespread application of this technique.

The combination of pre- and post-contrast T_1-mapping and 4D flow MRI allowed for a comprehensive structure-function assessment incorporating the quantification of ECV, outflow obstruction and LVOT hemodynamics. Specifically, the full 3D coverage afforded by 4D flow MRI allowed for the volumetric quantification of peak systolic pressure gradient based on the detection of peak velocity in the entire LVOT; an advantage compared to the

limited coverage of standard 2D PC MRI techniques which may results on peak velocity underestimation as demonstrated previously (40). Furthermore, assessment of combined ECV and LVOT hemodynamics is not possible with echocardiography. Thus, for patients where diagnosis of HCM severity is inconclusive on echocardiography, an additional MRI examination including T1-mapping and 4D flow MRI may be beneficial. Also, since HCM is a hereditary disease, MRI examinations in family members of HCM patients may detect the onset of the disease earlier than echocardiography. In these subjects where the severity of the disease has yet to establish, relatively long analysis times of the T1-mapping and 4D flow MRI data do not pose a problem.

This pilot study included a relatively small number of subjects and T_1-mapping or hematocrit was not available in all patients. In addition, T_1-mapping MRI was not performed in control subjects. Nevertheless, significant relationships between metrics of LVOT hemodynamic and ECV indicate the potential of 4D flow MRI and T1 mapping for the evaluation of changes in cardiac out-flow and tissue structure in HCM patients.

Conventional echocardiography and Doppler echo parameters were not obtained in our study cohort at the time of MR imaging. We were thus not able to investigate correlations between both modalities which could provide a better cross-modality understanding.

Late Gadolinium Enhancement (LGE) scans to distinguish between focal and diffuse myocardial fibrosis were not performed. Brouwer et al. combined LGE and T1-mapping measurements to quantify diffuse fibrosis and showed that there was no significant difference between HCM patients and controls (41). Thus, the increased ECV in HCM disease may not be a result of increased diffuse fibrosis, but a result of increased focal fibrosis. By not performing LGE measurements in this study, we did not have the possibility to show a similar relationship.

A further drawback of 4D flow MRI is related to limited spatial and temporal resolution which may lead to underestimation of peak blood flow velocities due to partial volume effects and/or temporal filtering (42). As a result, derived parameters such as peak systolic pressure gradient and energy loss $E_L^{'}$ may also be underestimated. Nevertheless the spatio-temporal resolution was similar for all subjects included in this study and relative differences between cohorts (patients versus controls) or associations (hemodynamic metrics vs ECV) are expected to be preserved.

The computation of peak systolic LVOT energy loss $E_L^{'}$ requires accurate 3D vessel segmentation. Since $E_L^{'}$ is calculated using the spatial derivatives of the flow field, minor differences in segmentation can lead to $E_L^{'}$ differences between observers, as expressed by the 15% intra- and inter-observer errors for $E_L^{'}$. Based on these findings, a power analysis indicates that the intra and inter-observer variability still allows for the detection of differences in $E_L^{'}$ of ≈0.75mW with a statistical power of 0.8 and $P<0.05$. These minimum detectable $E_L^{'}$ changes are clearly beyond the observed peak systolic $E_L^{'}$ differences between

cohorts (patients versus controls) detected in this study (3.8±2.5mW versus 1.5±0.7mW, respectively)

In conclusion, the combined application of pre- and post-contrast T_1-mapping and 4D flow MRI allows for the characterization of altered hemodynamics and myocardial ECV in patients with HCM. The correlation of peak systolic LVOT pressure gradient and energy loss $E_L^{'}$ with ECV indicates a possible mechanistic link between HCM-related flow abnormalities, increased LV afterload, and LV structural remodeling.

Acknowledgments

This work was supported by the National Institute of Health (NIH) National Heart, Lung, and Blood Institute (NHLBI) grants R01HL115828, K25HL119608

References

1. Elliott PM, Anastasakis A, Borger MA, et al. 2014 ESC Guidelines on diagnosis and management of hypertrophic cardiomyopathy: the Task Force for the Diagnosis and Management of Hypertrophic Cardiomyopathy of the European Society of Cardiology (ESC). Eur Heart J. 2014; 35(39):2733–2779. [PubMed: 25173338]
2. Gersh BJ, Maron BJ, Bonow RO, et al. 2011 ACCF/AHA Guideline for the Diagnosis and Treatment of Hypertrophic Cardiomyopathy: a report of the American College of Cardiology Foundation/American Heart Association Task Force on Practice Guidelines. Developed in collaboration with the American Association for Thoracic Surgery, American Society of Echocardiography, American Society of Nuclear Cardiology, Heart Failure Society of America, Heart Rhythm Society, Society for Cardiovascular Angiography and Interventions, and Society of Thoracic Surgeons. J Am Coll Cardiol. 2011; 58(25):e212–260. [PubMed: 22075469]
3. Maron BJ, Maron MS. Hypertrophic cardiomyopathy. The Lancet. 2013; 381(9862):242–255.
4. Braunwald E, Lambrew CT, Rockoff SD, Ross J Jr, Morrow AG. Idiopathic Hypertrophic Subaortic Stenosis. I. A Description of the Disease Based Upon an Analysis of 64 Patients. Circulation. 1964; 30(SUPPL 4):3–119. [PubMed: 14227306]
5. Henry WL, Clark CE, Griffith JM, Epstein SE. Mechanism of left ventricular outlfow obstruction in patients with obstructive asymmetric septal hypertrophy (idiopathic hypertrophic subaortic stenosis). Am J Cardiol. 1975; 35(3):337–345. [PubMed: 1167730]
6. Sherrid MV, Gunsburg DZ, Moldenhauer S, Pearle G. Systolic anterior motion begins at low left ventricular outflow tract velocity in obstructive hypertrophic cardiomyopathy. Journal of the American College of Cardiology. 2000; 36(4):1344–1354. [PubMed: 11028493]
7. Williams LK, Rakowski H. Surgical myectomy for hypertrophic obstructive cardiomyopathy: the cut that heals. Circulation. 2013; 128(3):193–197. [PubMed: 23770749]
8. Maron BJ. Hypertrophic cardiomyopathy: a systematic review. JAMA. 2002; 287(10):1308–1320. [PubMed: 11886323]
9. St John Sutton MG, Lie JT, Anderson KR, O'Brien PC, Frye RL. Histopathological specificity of hypertrophic obstructive cardiomyopathy. Myocardial fibre disarray and myocardial fibrosis. Br Heart J. 1980; 44(4):433–443. [PubMed: 7191711]
10. Choudhury L, Mahrholdt H, Wagner A, et al. Myocardial scarring in asymptomatic or mildly symptomatic patients with hypertrophic cardiomyopathy. Journal of the American College of Cardiology. 2002; 40(12):2156–2164. [PubMed: 12505229]
11. Araujo AQ, Arteaga E, Ianni BM, et al. Relationship between outflow obstruction and left ventricular functional impairment in hypertrophic cardiomyopathy: a Doppler echocardiographic study. Echocardiography. 2006; 23(9):734–740. [PubMed: 16999691]
12. Baumgartner H, Hung J, Bermejo J, et al. Echocardiographic assessment of valve stenosis: EAE/ASE recommendations for clinical practice. J Am Soc Echocardiogr. 2009; 22(1):1–23. quiz 101–102. [PubMed: 19130998]

13. Ho CY, Lopez B, Coelho-Filho OR, et al. Myocardial fibrosis as an early manifestation of hypertrophic cardiomyopathy. N Engl J Med. 2010; 363(6):552–563. [PubMed: 20818890]
14. Ellims AH, Iles LM, Ling LH, et al. A comprehensive evaluation of myocardial fibrosis in hypertrophic cardiomyopathy with cardiac magnetic resonance imaging: linking genotype with fibrotic phenotype. Eur Heart J Cardiovasc Imaging. 2014; 15(10):1108–1116. [PubMed: 24819852]
15. Lindman BR, Bonow RO, Otto CM. Current management of calcific aortic stenosis. Circ Res. 2013; 113(2):223–237. [PubMed: 23833296]
16. Allen BD, Choudhury L, Barker AJ, et al. Three-dimensional haemodynamics in patients with obstructive and non-obstructive hypertrophic cardiomyopathy assessed by cardiac magnetic resonance. Eur Heart J Cardiovasc Imaging. 2015; 16(1):29–36. [PubMed: 25108915]
17. Pibarot P, Garcia D, Dumesnil JG. Energy loss index in aortic stenosis: from fluid mechanics concept to clinical application. Circulation. 2013; 127(10):1101–1104. [PubMed: 23479666]
18. Venkatachari AK, Halliburton SS, Setser RM, White RD, Chatzimavroudis GP. Noninvasive quantification of fluid mechanical energy losses in the total cavopulmonary connection with magnetic resonance phase velocity mapping. Magn Reson Imaging. 2007; 25(1):101–109. [PubMed: 17222721]
19. Barker AJ, van Ooij P, Bandi K, et al. Viscous energy loss in the presence of abnormal aortic flow. Magn Reson Med. 2014; 72(3):620–628. [PubMed: 24122967]
20. Moon JC, Messroghli DR, Kellman P, et al. Myocardial T1 mapping and extracellular volume quantification: a Society for Cardiovascular Magnetic Resonance (SCMR) and CMR Working Group of the European Society of Cardiology consensus statement. J Cardiovasc Magn Reson. 2013; 15:92. [PubMed: 24124732]
21. Dass S, Suttie JJ, Piechnik SK, et al. Myocardial tissue characterization using magnetic resonance noncontrast t1 mapping in hypertrophic and dilated cardiomyopathy. Circ Cardiovasc Imaging. 2012; 5(6):726–733. [PubMed: 23071146]
22. Banypersad SM, Sado DM, Flett AS, et al. Quantification of Myocardial Extracellular Volume Fraction in Systemic AL Amyloidosis An Equilibrium Contrast Cardiovascular Magnetic Resonance Study. Circulation: Cardiovascular Imaging. 2013; 6(1):34–39. [PubMed: 23192846]
23. Bull S, White SK, Piechnik SK, et al. Human non-contrast T1 values and correlation with histology in diffuse fibrosis. Heart. 2013; 99(13):932–937. [PubMed: 23349348]
24. Coelho-Filho OR, Shah RV, Mitchell R, et al. Quantification of cardiomyocyte hypertrophy by cardiac magnetic resonance: implications for early cardiac remodeling. Circulation. 2013; 128(11): 1225–1233. [PubMed: 23912910]
25. Puntmann VO, Voigt T, Chen Z, et al. Native T1 Mapping in Differentiation of Normal Myocardium From Diffuse Disease in Hypertrophic and Dilated Cardiomyopathy. JACC: Cardiovascular Imaging. 2013; 6(4):475–484. [PubMed: 23498674]
26. Ho CY, Abbasi SA, Neilan TG, et al. T1 measurements identify extracellular volume expansion in hypertrophic cardiomyopathy sarcomere mutation carriers with and without left ventricular hypertrophy. Circ Cardiovasc Imaging. 2013; 6(3):415–422. [PubMed: 23549607]
27. Wigstrom L, Sjoqvist L, Wranne B. Temporally resolved 3D phase-contrast imaging. Magn Reson Med. 1996; 36(5):800–803. [PubMed: 8916033]
28. Messroghli DR, Greiser A, Frohlich M, Dietz R, Schulz-Menger J. Optimization and validation of a fully-integrated pulse sequence for modified look-locker inversion-recovery (MOLLI) T1 mapping of the heart. J Magn Reson Imaging. 2007; 26(4):1081–1086. [PubMed: 17896383]
29. Kellman P, Wilson JR, Xue H, et al. Extracellular volume fraction mapping in the myocardium, part 2: initial clinical experience. J Cardiovasc Magn Reson. 2012; 14:64. [PubMed: 22967246]
30. Kellman P, Wilson JR, Xue H, Ugander M, Arai AE. Extracellular volume fraction mapping in the myocardium, part 1: evaluation of an automated method. J Cardiovasc Magn Reson. 2012; 14:63. [PubMed: 22963517]
31. Bock, J.; Kreher, B.; Hennig, J.; Markl, M. Optimized pre-processing of time-resolved 2D and 3D phase contrast MRI data. Proceedings of the 15th Annual Meeting of ISMRM; Berlin, Germany. 2007; p. 3138

32. Quinones MA, Otto CM, Stoddard M, et al. Recommendations for quantification of Doppler echocardiography: a report from the Doppler Quantification Task Force of the Nomenclature and Standards Committee of the American Society of Echocardiography. Journal of the American Society of Echocardiography: official publication of the American Society of Echocardiography. 2002; 15(2):167–184. [PubMed: 11836492]

33. Bird, RB.; Stewart, WE.; Lightfoot, EN. Transport Phenomena. New York: John Wiley and Sons, Inc; 1960.

34. Miller CA, Naish JH, Bishop P, et al. Comprehensive validation of cardiovascular magnetic resonance techniques for the assessment of myocardial extracellular volume. Circ Cardiovasc Imaging. 2013; 6(3):373–383. [PubMed: 23553570]

35. Kehr E, Sono M, Chugh S, Jerosch-Herold M. Gadolinium-enhanced magnetic resonance imaging for detection and quantification of fibrosis in human myocardium in vitro. The International Journal of Cardiovascular Imaging. 2008; 24(1):61–68. [PubMed: 17429755]

36. Bahlmann E, Cramariuc D, Gerdts E, et al. Impact of pressure recovery on echocardiographic assessment of asymptomatic aortic stenosis: a SEAS substudy. JACC Cardiovasc Imaging. 2010; 3(6):555–562. [PubMed: 20541709]

37. Schnell S, Markl M, Entezari P, et al. k-t GRAPPA accelerated four-dimensional flow MRI in the aorta: effect on scan time, image quality, and quantification of flow and wall shear stress. Magn Reson Med. 2014; 72(2):522–533. [PubMed: 24006309]

38. Basha TA, Akcakaya M, Goddu B, Berg S, Nezafat R. Accelerated three-dimensional cine phase contrast imaging using randomly undersampled echo planar imaging with compressed sensing reconstruction. NMR Biomed. 2015; 28(1):30–39. [PubMed: 25323208]

39. Tariq U, Hsiao A, Alley M, Zhang T, Lustig M, Vasanawala SS. Venous and arterial flow quantification are equally accurate and precise with parallel imaging compressed sensing 4D phase contrast MRI. J Magn Reson Imaging. 2013; 37(6):1419–1426. [PubMed: 23172846]

40. Nordmeyer S, Riesenkampff E, Messroghli D, et al. Four-dimensional velocity-encoded magnetic resonance imaging improves blood flow quantification in patients with complex accelerated flow. J Magn Reson Imaging. 2013; 37(1):208–216. [PubMed: 22976284]

41. Brouwer WP, Baars EN, Germans T, et al. In-vivo T1 cardiovascular magnetic resonance study of diffuse myocardial fibrosis in hypertrophic cardiomyopathy. Journal of Cardiovascular Magnetic Resonance. 2014; 16(28)10.1186/1532-1429X-1116-1128

42. Hamilton CA. Correction of partial volume inaccuracies in quantitative phase contrast MR angiography. Magnetic Resonance Imaging. 1994; 12(7):1127–1130. [PubMed: 7997100]

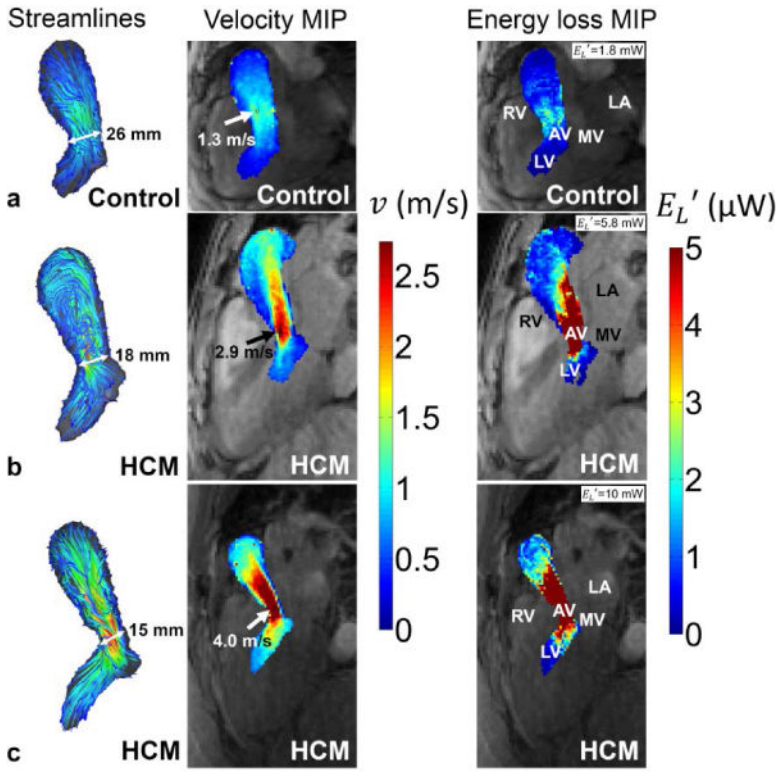

Figure 1.

Peak systolic 3D streamlines (left column), velocity maximum intensity projections (mid column) and E_L' maximum intensity projections (right column) in the LVOT of (a) a control subject, (b) a HCM patient with helical flow and (c) a HCM patient with obstructed flow. The arrows point to the location of maximum velocity used for Bernoulli pressure gradient estimation. End diastolic LVOT diameters were smallest for the obstructive HCM patient (15 mm) compared to the HCM patient with helical flow (18 mm) and the age matched healthy control (26 mm). Note that the color coding of the maximum velocity (red color) corresponds to a pressure gradient of 30 mmHg. RV = right ventricle, AV = aortic valve, LA = left atrium, MV = mitral valve, LV = left ventricle.

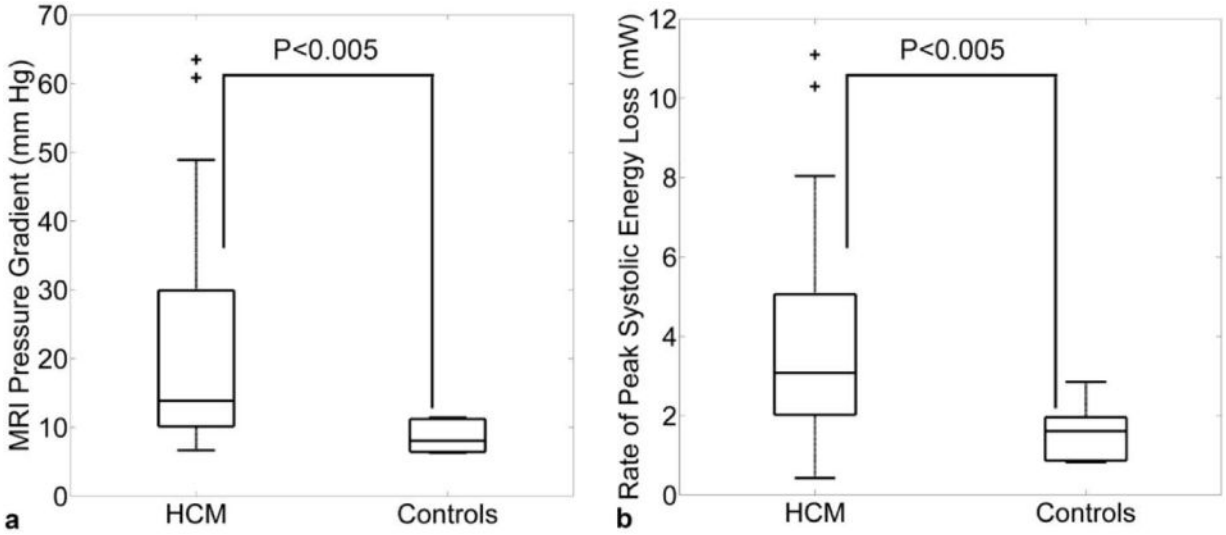

Figure 2.

(a) Estimated peak systolic LVOT Bernoulli pressure gradients and (b) LVOT peak systolic energy loss due to viscous dissipation $E_L^{'}$ in HCM patients and age matched normal controls. The individual box plots illustrate the median and the 25th and 75th percentiles (edges), the whiskers extend to the most extreme data points not considered outliers, outliers are plotted individually as '+'.

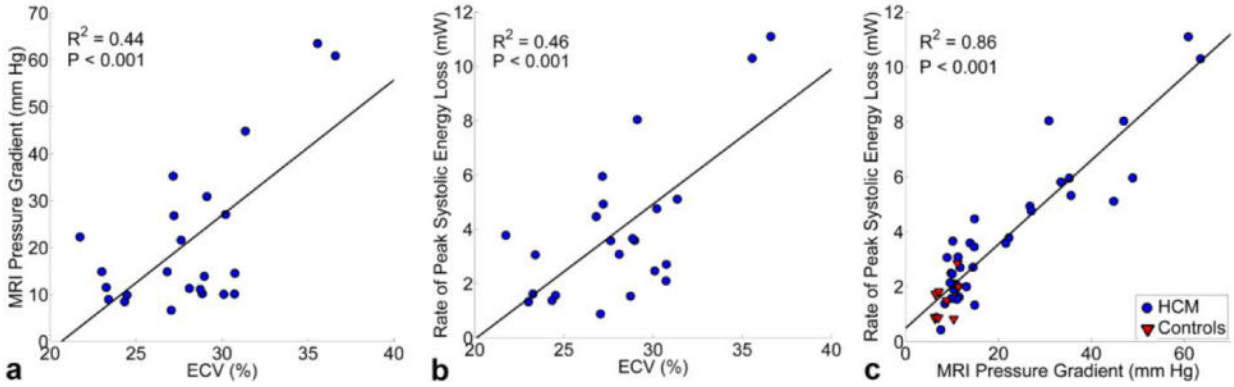

Figure 3.

Linear regression analysis between left ventricular ECV and (a) peak systolic LVOT Bernoulli pressure gradients and (b) LVOT peak systolic energy loss E_L' in HCM patients (n=23). (c) Correlation between peak systolic E_L' and pressure gradient in all HCM patients (n=35) and age matched controls (n=10).

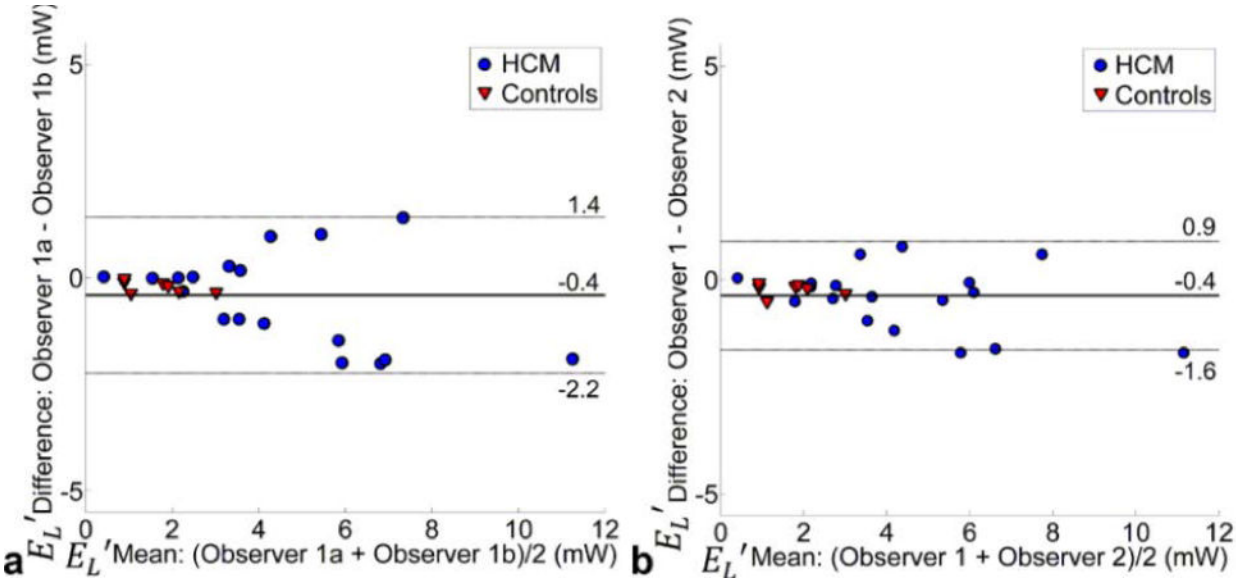

Figure 4.

Bland-Altman analysis of (a) intra-and (b) inter-observer variability of E_L' in a subgroup of n=25 subjects.

Table 1

HCM patient characteristics

	Patients	Controls	P*
age [years]	53.8 ± 15.3	44.9 ± 13.9	0.07
gender [male/female]	25/10	6/4	–
septal thickness [mm]	18.9 ± 5.3	10.8 ± 1.8	<0.001
free wall thickness [mm]	11.2 ± 2.8	9.8 ± 1.2	0.16
Septal/posterior wall thickness ratio	1.8 ± 0.7	1.1 ± 0.3	<0.001
LVOT diameter [mm]	21.5 ± 3.3	24.3 ± 1.9	0.007
Presence of SAM	22 of 35 (63%)	0 of 10 (0%)	–

*Wilcoxon rank sum test, P<0.05 considered significant

Table 2

ECV and results of correlation analysis with pressure gradient and E_L' for n=23 in HCM patients who underwent both 4D flow MRI and pre- and post-contrast T_1-mapping.

		LVOT pressure gradient		LVOT energy loss	
	Mean ECV (%)	**R^2**	**P**	**R^2**	**P**
entire LV[1]	28 ± 4	0.44	<0.001	0.46	<0.001
Septum[2]	29 ± 4	0.38	<0.01	0.42	<0.001
Free Wall[3]	26 ± 4	0.34	<0.01	0.31	<0.01
P-value	0.14[*]		–		

[1] n=23, in 2 patients ECV was averaged over base and mid due to insufficient image quality in the apex

[2] n=23, for 5 subjects ECV was averaged over base and mid due to insufficient image quality in the apex

[3] n=22, ECV calculation was not feasible for 1 patient due to insufficient image quality, for 5 subjects ECV was averaged over base and mid due to insufficient image quality in the apex

[*] Difference between ECV values for entire LV, Septum and Free Wall, Kruskal-Wallis test, significant when P<0.05

Table 3

Linear regression relationships between the pressure gradient and E_L' and ECV, septal thickness, septal/posterior wall thickness ratio, presence of SAM and LVOT diameter. Results in bold type indicate significant relationships.

		LVOT structure							
		Septal Thickness (mm)		Septal/posterior wall thickness ratio		Presence of SAM		LVOT diameter (mm)	
		R^2	P	R^2	P	R^2	P	R^2	P
LVOT hemodynamics	**pressure gradient**	0.00	0.72	0.04	0.28	**0.12**	**<0.05**	**0.14**	**<0.05**
	E_L'	0.00	0.86	0.05	0.19	0.05	0.20	0.07	0.14